Available online at www.sciencedirect.com
ScienceDirect
Journal of Solid State Chemistry 180 (2007) 2830–2837
JOURNAL OF SOLID STATE CHEMISTRY
www.elsevier.com/locate/jssc

Synthesis, structure and physical properties of the new uranium ternary phase $U_3Co_2Ge_7$

Svilen Bobev[a,*], Eric D. Bauer[b], Filip Ronning[b], Joe D. Thompson[b], John L. Sarrao[b]

[a]*Department of Chemistry and Biochemistry, University of Delaware, Newark, DE 19716, USA*
[b]*Materials Physics and Applications Division (MPA-10), Los Alamos National Laboratory, Los Alamos, NM 87545, USA*

Received 8 June 2007; received in revised form 30 July 2007; accepted 30 July 2007
Available online 25 August 2007

Abstract

A new ternary compound, $U_3Co_2Ge_7$, has been synthesized from the corresponding elements by a high temperature reaction using molten tin flux. It crystallizes in the orthorhombic $La_3Co_2Sn_7$-type (Pearson's symbol *oC*24, space group *Cmmm*, No. 65) with lattice parameters determined from single-crystal X-ray diffraction as follows: $a = 4.145(2)$ Å; $b = 24.920(7)$; $c = 4.136(2)$ Å, $V = 427.2(3)$ Å^3. Structure refinements confirm an ordered structure having two crystallographically inequivalent uranium atoms, occupying sites with dissimilar coordination. $U_3Co_2Ge_7$ orders ferromagnetically below 40 K and undergoes a consecutive magnetic transition at 20 K. These results have been obtained from temperature- and field-dependent magnetization, resistivity and heat-capacity measurements. The estimated Sommerfeld coefficient $\gamma = 87$ mJ/mol-U K^2 suggests $U_3Co_2Ge_7$ to be a moderately heavy-fermion material.

Keywords: Crystal structure; Heavy-fermions; $La_3Co_2Sn_7$; Magnetic measurements; $U_3Co_2Ge_7$; Uranium intermetallics

1. Introduction

A variety of uranium-containing intermetallic compounds have been extensively studied during the past 3–4 decades [1–6]. The interest in such materials has been largely fueled by the unusual temperature dependence of the specific heat (C_P) that leads to a very large value of C_P/T at low temperature (Sommerfeld coefficient or electronic component to the heat capacity, $\gamma = C_P/T$). Several well-known examples include UPt_3, UBe_{13}, UGe_2, UCd_{11}, U_2Zn_{17}, among others, illustrious for the rich heavy-fermion phenomenology they exhibit [7–11]. Today, it is commonly accepted that the anomalously large γ-values in these *U*-phases arises from hybridization of the 5*f*-electrons with *s*-, *p*- and *d*-electrons of the ligands, resulting in the formation of highly correlated bands near the Fermi level [6,12–14]. Recently, such bands were found to take part in the superconducting condensate as demonstrated on the examples of UGe_2 (itinerant ferromagnet) [7], URu_2Si_2 (hidden order antiferromagnet) [15], URhGe (field-induced re-entrant superconductor) [16], to name just a few. The latter compound is also regarded as the first bulk ferromagnetic superconductor at ambient pressure. Such unprecedented results have broad implications in various subfields of condensed-matter research and call the attention to new experimental studies to better understand the origin of unconventional superconductivity.

With these ideas in mind, we embarked on exploratory studies of new heavy-fermion materials in the systems U-*TM*-Ge and U-*TM*-Si, where *TM* stands for various mid-to-late transition metals. Unlike in previous studies, where arc- or induction-melting has been the synthetic method of choice, we employed the molten metal-flux method [17] in order to grow large single crystals and/or to synthesize metastable phases. With this paper, we report the synthesis, the structural characterization and the properties of a new ferromagnetic compound, $U_3Co_2Ge_7$, which one of the very few U-based phases with the orthorhombic $La_3Co_2Sn_7$ structure type (space group *Cmmm*, No. 65, Pearson's symbol *oC*24) [18,19]. The other two known examples are $U_3Fe_2Si_7$ and $U_3Co_2Si_7$ [20], however, they are incorrectly classified in the Pearson's handbook with their own type (dubbed $U_3Fe_2Si_7$, space group *Cmmm*, No. 65, Pearson's

*Corresponding author. Fax: +1 302 831 6335.
E-mail address: bobev@udel.edu (S. Bobev).

0022-4596/$ - see front matter © 2007 Elsevier Inc. All rights reserved.
doi:10.1016/j.jssc.2007.07.032

symbol *oC*24) [18]. In spite of this inconsistency in the older literature, these structures are isopointal and are known to have two unique U-sites with very different coordination—one at the center of a cubeoctahedron, analogous to that in UGe_3 ($AuCu_3$-type), and another one whose polyhedron resembles those of Ce in the orthorhombic $CeNiSi_2$-type [18]. Temperature- and field-dependent magnetization and resistivity measurements confirm that the 5*f*-electrons of the uranium atoms have neither pure itinerant nor pure localized character. These findings are corroborated by the temperature dependence of the heat capacity, which suggests $U_3Co_2Ge_7$ to be a moderate heavy-fermion compound in the ordered state.

2. Experimental

2.1. Synthesis

The starting materials, all with purity greater than 99.99% were used as received. A mixture of depleted U, Co and Ge in the stoichiometric ratio of 1:1:3 was loaded in an alumina crucible, together with a 20-fold excess of Sn (intended as a flux). The crucible was then placed in a fused silica ampoule, which was subsequently evacuated and flame-sealed. Reactions were carried out in a Lindberg muffle furnace at 1373 K for 4 h, followed by cooling to 873 K at a rate of 5°/h, whereupon the excess tin was removed and the samples were allowed to cool to room temperature. The reaction outcome consisted of thin, plate-like crystals, some up to 3–4 mm^3. Later, the majority of these were determined to be of the title compound. Single-crystal diffraction studies also confirmed the presence of $U_3Co_4Ge_7$ [21] as a minor phase.

The crystals of $U_3Co_2Ge_7$ had silver-metallic color. They are stable in air and moisture over periods of time greater than 6 months.

2.2. X-ray diffraction studies

X-ray powder diffraction patterns were taken on a Scintag XDS 2000 diffractometer with monochromatized Cu*K*α radiation ($\lambda = 1.5406$ Å) and up to a 2θ limit of 80°. The collected data were used for a phase identification, which was done using the JADE 6.5 package [22]. The intensity and the peak positions in the experimental powder patterns were in good agreement with those calculated from the structure as refined from single-crystal data (below). However, we point out that assessing the sample purity from powder data could not be considered very reliable. This is easy to understand if one recognizes that many of the Bragg peaks corresponding to $U_3Co_2Ge_7$ and to the side product $U_3Co_4Ge_7$ [21] overlap. Therefore, to ascertain the crystals used for the property measurements, all of them were checked and indexed using X-ray single-crystal diffraction.

Single-crystal X-ray diffraction was also used in order to unequivocally determine the crystal structure. To do so, several crystals were selected from the Sn-flux reactions, cut to suitable dimensions for data collection and checked for singularity. One of them was subsequently chosen (platelet, $0.04 \times 0.03 \times 0.03\,mm^3$) for an intensity data collection, which was carried out on a Bruker SMART CCD single-crystal diffractometer with monochromatized Mo*K*α radiation. Since the crystal was mounted on a glass fiber utilizing Paratone N Oil, a low temperature data acquisition was deemed more appropriate. It was done in 4 batch runs with 0.4° ω-scans, 15 s per frame, $2\theta_{max} = 56.4°$, covering a full sphere of reciprocal space. The Bruker-supplied SMART and SAINT software packages [23] were used for the data collection, indexing, reduction and integration. Semi-empirical absorption correction based on equivalents was applied with the aid of SADABS [24]. Inspection of the reciprocal space did not provide any evidence for data ($I > 2\sigma_{(I)}$), which violate the reflections' conditions or for twinning.

The structure was solved by direct-methods in *Cmmm* (No. 65) and refined on F^2 with SHELX [25]. At this point, it was recognized that $U_3Co_2Ge_7$ is a new member of the $La_3Co_2Sn_7$ type (Pearson's symbol *oC*24) [18,19], and for the sake of uniformity, the atomic coordinates and the labeling scheme from $La_3Co_2Sn_7$ were adopted (we noted already an inconsistency in the older literature—the $U_3Fe_2Si_7$ and the $U_3Co_2Si_7$ structures [20] are not assigned with the $La_3Co_2Sn_7$ type, although they are isostructural). Refinements of the structure showed no indications that the occupancies of the U, Co, or Ge sites deviate from full—when the site occupation factor of an individual atom was freed to vary while the remaining ones were kept fixed, all deviations from full occupancy were within 3σ. Despite the fact that the $U_3Co_2Ge_7$ crystals were grown in Sn flux, there is no evidence to suggest Sn inclusions or substitutions. This is particularly worth noting because the archetype $La_3Co_2Sn_7$ is a Sn-based compound and excluding $Ce_3Ni_2Ge_7$ [26] there are no other structurally characterized germanides that crystallize with this structure.

In the last refinement cycles, all atoms were refined with anisotropic displacement parameters. The final Fourier map is flat—both the highest residual density and deepest hole (ca. $\pm 3\ e^-/Å^3$) are located approximately 1.5 Å away from Ge4. Additional details of the data collection and structure refinements are given in Table 1. Positional and equivalent isotropic displacement parameters, and relevant interatomic distances are listed in Tables 2 and 3, respectively. Further details on the crystal structure investigations can be obtained from the Fachinformations-zentrum Karlsruhe, 76344 Eggenstein-Leopoldshafen, Germany, (fax: (49) 7247 808 666; e-mail: crysdata@fiz.karlsruhe.de) on quoting the depository number CSD 418093.

2.3. Physical property measurements

Magnetization measurements were performed in a Quantum Design MPMS-7 SQUID magnetometer from

Table 1
Selected single-crystal X-ray diffraction data collection and refinement parameters for $U_3Co_2Ge_7$

Chemical formula	$U_3Co_2Ge_7$
Formula weight	1340.08
Crystal system	Orthorhombic
Space group, Z	*Cmmm* (No. 65), 2
Temperature	120(2) K
Unit cell parameters	$a = 4.145(2)$ Å $b = 24.920(7)$ Å $c = 4.136(2)$ Å $V = 427.2(3)$ Å^3
Radiation, λ	Mo$K\alpha$, 0.71073 Å
ρ_{calc}	10.416 g/cm^3
2θ limit	56.4°
Absorption coefficient	84.523 cm^{-1}
Collected/unique reflections/R_{int}	1589/336/0.0411
Data ($I>2\sigma_{(I)}$)/restraints/parameters	282/0/28
Goodness-of-fit on F^2	1.022
Final R indices ($I>2\sigma_{(I)}$)[a]	$R_1 = 0.0356$ w$R_2 = 0.0775$
Extinction coefficient	0.0028(2)
Largest diff. peak and hole	+3.12/–3.27 e$^-$/Å^3

[a] $R_1 = \sum||F_o|-|F_c||/\sum|F_o|$; $wR_2 = [\sum[w(F_o^2-F_c^2)^2]/\sum[w(F_o^2)^2]]^{1/2}$, and $w = 1/[\sigma^2F_o^2 + (0.047P)^2]$, $P = (F_o^2 + 2F_c^2)/3$.

Table 2
Atomic coordinates, equivalent isotropic displacement parameters (U_{eq})[a] for $U_3Co_2Ge_7$

Atom	Wyckoff	x	y	z	U_{eq} (Å^2)
U1	2*c*	1/2	0	1/2	0.0075(4)
U2	4*i*	0	0.1842(1)	0	0.0078(3)
Co	4*j*	0	0.3711(1)	1/2	0.0090(7)
Ge1	2*a*	0	0	0	0.0083(7)
Ge2	4*i*	0	0.4124(1)	0	0.0097(6)
Ge3	4*j*	0	0.0875(1)	1/2	0.0098(6)
Ge4	4*j*	0	0.2790(1)	1/2	0.0087(6)

[a] U_{eq} is defined as one-third of the trace of the orthogonalized U_{ij} tensor.

Table 3
Selected interatomic distances in $U_3Co_2Ge_7$

Atom pair	Distance (Å)	Atom pair	Distance (Å)
U1–Ge1 × 4	2.928(1)	Ge1–U1 × 4	2.928(1)
U1–Ge2 × 4	3.007(2)	Ge2–Co × 2	2.310(2)
U1–Ge3 × 4	3.009(2)	Ge2–Ge3 × 4	2.928(1)
U1–Co × 2	3.213(3)	Ge3–Co × 2	2.315(2)
		Ge3–Ge2 × 4	2.928(1)
U2–Ge4 × 4	3.068(1)	Ge4–Co	2.295(4)
U2–Ge4 × 2	3.139(2)	Ge4–Ge4 × 2	2.526(3)
U2–Ge3 × 2	3.176(2)	Co–Ge4	2.295(4)
U2–Ge2 × 2	3.177(2)	Co–Ge2 × 2	2.310(2)
U2–Co × 4	3.236(2)	Co–Ge3 × 2	2.315(2)

1.8 to 350 K in magnetic fields up to 6.5 T. Flux-grown single crystals of $U_3Co_2Ge_7$ were secured between pieces of quartz wool and suspended in a low background sample holder. The crystal orientation was such that the magnetic field was parallel to the principal axis of the crystal (assumed to be the longest crystallographic axis but not confirmed by diffraction). Raw data were corrected for diamagnetic contribution from the holder and converted to magnetic susceptibility in emu/mol units. Specific heat $C_p(T)$ data were obtained on a custom-designed system using the adiabatic method in the temperature range 2–300 K. Measurements of the electrical resistivity as a function of the temperature (also from 2 to 300 K) were performed using a LR-700 resistance bridge. The four-probe technique with an excitation current of 1 mA was used. For that purpose, four 0.002″ platinum wires were attached to the sample by spot-welding. For all data reported herein, polished single crystals were used to minimize geometric and contact-resistance errors.

3. Results and discussion

3.1. Structure

$U_3Co_2Ge_7$ is the sixth structurally characterized compound in the U–Co–Ge system, after UCoGe [27], UCo_2Ge_2 (two polymorphs) [28], UCo_6Ge_6 [29], $U_2Co_{15}Ge_2$ [30], and $U_3Co_4Ge_7$ [21]. It crystallizes with the known $La_3Co_2Sn_7$ type [18,19], and there are 2 uranium, 1 cobalt and 4 germanium atoms in the asymmetric unit, all in special positions (Table 2). Since this structure is made up of fragments that are very common amongst the intermetallic phases [18], herein, we focus our attention on the coordination of the U-atoms in conjunction with the physical properties. The close structural relationship between the new $U_3Co_2Ge_7$ phase and the recently reported $U_3Co_4Ge_7$ [21] is emphasized as well. A perspective view of the structure (viewed approximately down the *c*-axis) is shown in Fig. 1a; relevant positional parameters and interatomic distance are given in Tables 2 and 3, respectively.

In this structure, there are two crystallographically unique positions for the uranium atoms with site symmetry of *mmm* and *m2m*, labeled U1 and U2, respectively (Table 2). As shown in Fig. 1b, the U1 atoms are positioned at the centers of truncated cubes (cube-octahedra) of Ge atoms. Two opposing faces of the truncated cubes are capped by Co atoms (along the direction of the crystallographic *b*-axis), bringing the total coordination number to 14. The other type of U atoms, U2, also have CN 14 but their polyhedra differ markedly from those of U1. U2 can be viewed as located near the center of a distorted hexagonal prism made of 4 cobalt and 8 germanium atoms, two adjacent faces of which are capped by germanium atoms (Fig. 1c). We point out that not only the shape of the polyhedra are different but also are the average U–Ge distances, for example d_{U1-Ge} vary from 2.928(1) to 3.009(2) Å, while the corresponding d_{U2-Ge} are almost 0.15 Å longer (Table 3). These contacts lie well within the range of U–Ge distances reported for other binary and ternary uranium germanides [21,27–31]. The dissimilar coordination, and more specifically—the

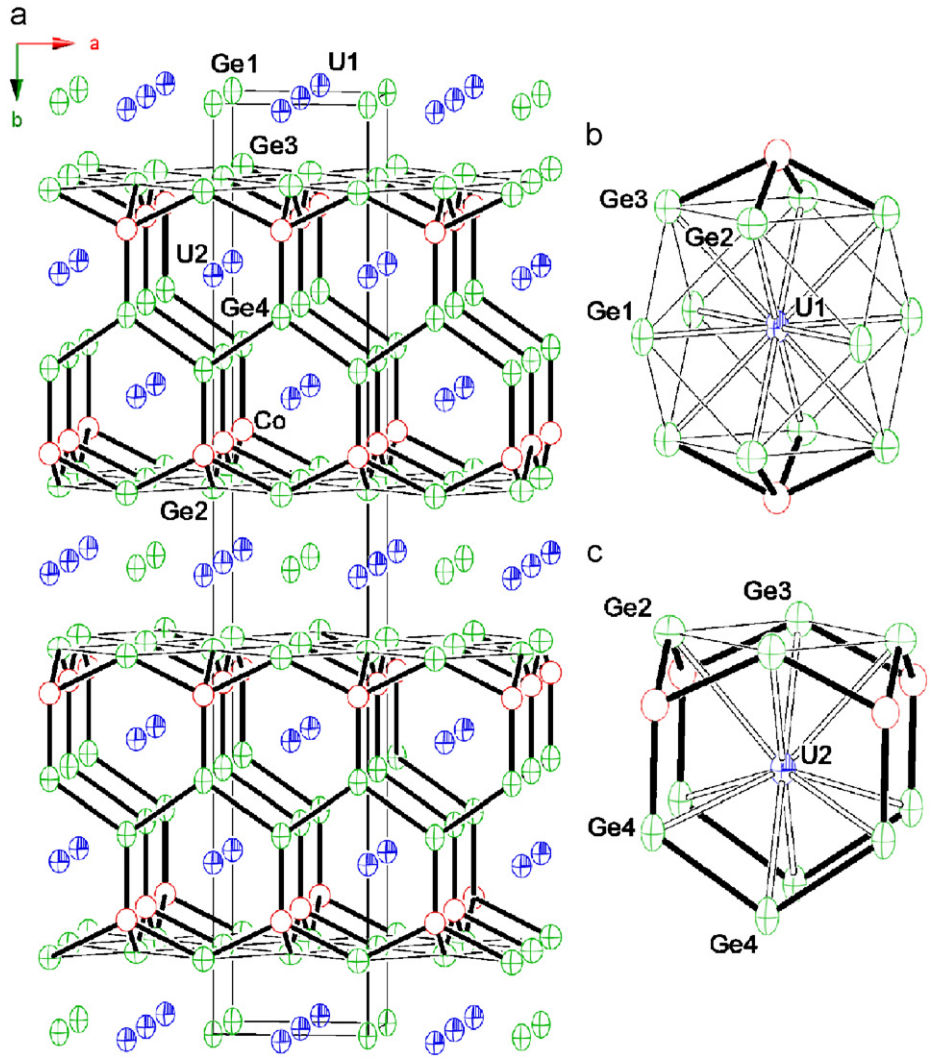

Fig. 1. (a) The orthorhombic structure $U_3Co_2Ge_7$ ($La_3Co_2Sn_7$-type), viewed approximately down the *c*-axis. Anisotropic displacement parameters are depicted at the 90% probability level: U atoms are shown with full thermal ellipsoids, Ge atoms are represented with crossed ellipsoids and the Co atoms are drawn with open circles. Unit cell is outlined. Views of the U1 and U2 coordination polyhedra are shown in (b) and (c), respectively. Online color: U—blue, Ge—green, Co—red.

shorter distances around the 2*c* cationic site (U1 in this case) has been noted on the example of the isostructural $Ce_3Ni_2Ge_7$ and has been suggested to be directly related to the intermediate valence of the Ce1 atoms in this material [26]. Discussion based on a similar line of thoughts has been given for the structurally related $U_3Co_4Ge_7$ as well [21].

Another important difference between the two types of uranium atoms is in their spatial arrangement with respect to each other—U1 atoms form nearly square-planar layers perpendicular to the direction of the crystallographic *b*-axis (Fig. 1a), with U1–U1 separation equal to the length of the *a*- and *c*-axis, respectively. U2 atoms, in turn, form ca. 3.4 Å-thick slabs of faced-shared triangular prisms. These prisms share triangular faces in direction parallel to the direction of the crystallographic *c*-axis and two of their rectangular faces in direction parallel to the direction of the *a*-axis, resulting in U2–U2 separation of 3.878(2) Å (compared to ca. 4.14 Å for d_{U1-U1}). Such distances are much longer than the distances in elemental U [32]; they are greater than the Hill criteria of 3.4 Å [33], indicating weak U–U interactions.

An interesting aspect of the $U_3Co_2Ge_7$ structure is its close structural relationship with that of $U_3Co_4Ge_7$ [21], which is shown in a side-by-side comparison in Fig. 2. The structure of $U_3Co_4Ge_7$ (*I*4/*mmm*, $a \approx 4.11$; $c \approx 27.48$ Å) is described as an intergrowth of UCo_2Ge_2 ($CaBe_2Ge_2$ type) and UGe_3 ($AuCu_3$ type) [18]. The structure of $U_3Co_2Ge_7$ (*Cmmm*, $a \approx c \approx 4.14$; $b \approx 24.92$ Å) is evidently very similar and can be formally derived from that of $U_3Co_4Ge_7$ by removing two layers of Co (roughly at 1/3 and 2/3 of the longest axis in Fig. 2-left), followed by an appropriate unit cell re-scaling and reconstruction, with a concomitant small orthorhombic distortion. The topology of the resultant slab $UCoGe_2$ is exactly that of the orthorhombic $CeNiSi_2$ type [18]. According to this, the formula unit of $U_3Co_2Ge_7$

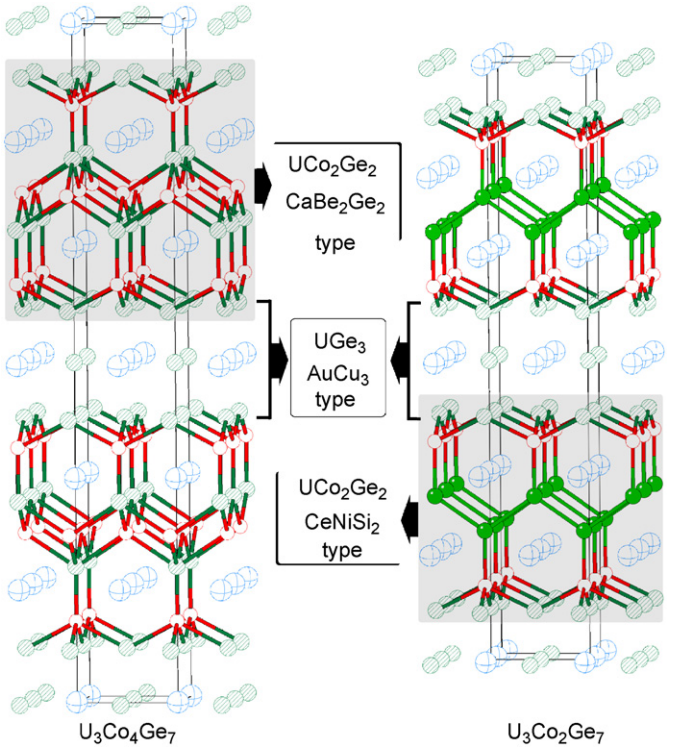

Fig. 2. Schematic representation of the close structural relationship between the body-centered tetragonal $U_3Co_4Ge_7$ (Ref. [19]) and the base-centered orthorhombic $U_3Co_2Ge_7$ (this work). Color code as in Fig. 1. Both structures can be considered as intergrowths of fragments of ubiquitous types—$AuCu_3$, $CaBe_2Ge_2$ and $CeNiSi_2$. See text for details.

can be then broken down as follows:

$$U_3Co_2Ge_7 = 2 \times UCoGe_2 + UGe_3.$$

It is therefore conceivable that of $U_3Co_2Ge_7$ and $U_3Co_4Ge_7$ are members of a potentially large series of homologs, the structures of which share similar building blocks. If this is the case, such principles can be applied in a broader context and be used as guide to make reasonable predictions about the composition and the possible structure of new, hitherto unknown compounds. For example, if one were to "assemble" slabs of UGe_3 ($AuCu_3$ type), $UCoGe_2$ ($CeNiSi_2$ type), and UCo_2Ge_2 ($CaBe_2Ge_2$ type) into one structure, it would have a composition $U_3Co_3Ge_7$ and is predicted to have a very long repeating unit (ca. 50 Å) along the direction of the stacking sequence. Whether or not such compound can be synthesized is yet to be found; however, we note that similar design of homologs is not unprecedented in the solid-state chemistry of the silicides and germanides, and there are several known series, such as $RE_{2n+1}Ge_{3n+2}$ ($n = 0, 1, 2\ldots\infty$) [34]; $RE[AuAl_2]_nAl_2(Au_xSi_{1-x})_2$ (RE = rare-earth metal) [35], $U_nCo_{6(n-m)}Si_{3n+2(m-1)}$ [36], among others.

3.2. Physical properties

Fig. 3a shows a plot of the zero field cooled magnetic susceptibility (χ) versus temperature (T), obtained on a single-crystalline specimen of $U_3Co_2Ge_7$. As illustrated in the inset, the high temperature data ($100 < T < 350$ K) is well fit by the modified Curie–Weiss law $\chi = \chi_0 + C/(T-\Theta_{CW})$, where C is the Curie constant and Θ_{CW} is the Curie–Weiss temperature. The use of the modified Curie–Weiss law was needed in order to account for possible ferromagnetic fluctuations. From the fit, the following parameters were obtained: $\chi_0 = 0.008$ emu/mol U, $\Theta_{CW} = 33$ K, and $C = N_A\mu_{eff}^2/3k_B = 0.727$, where N_A is the Avogadro's constant and k_B is the Boltzmann constant. Thereby, an effective paramagnetic moment of $\mu_{eff} = 2.41\,\mu_B$ was calculated. Such value, however, is lower than the expected moment for a free uranium in either f^2 or f^3 configuration, which would give $\mu_{eff} = 3.58\,\mu_B$ and $\mu_{eff} = 3.62$, respectively [34]. We also note that while it is possible that the effective moment could show some anisotropy at these temperatures (i.e., one would expect full recovery of the effective moment at higher tempera-

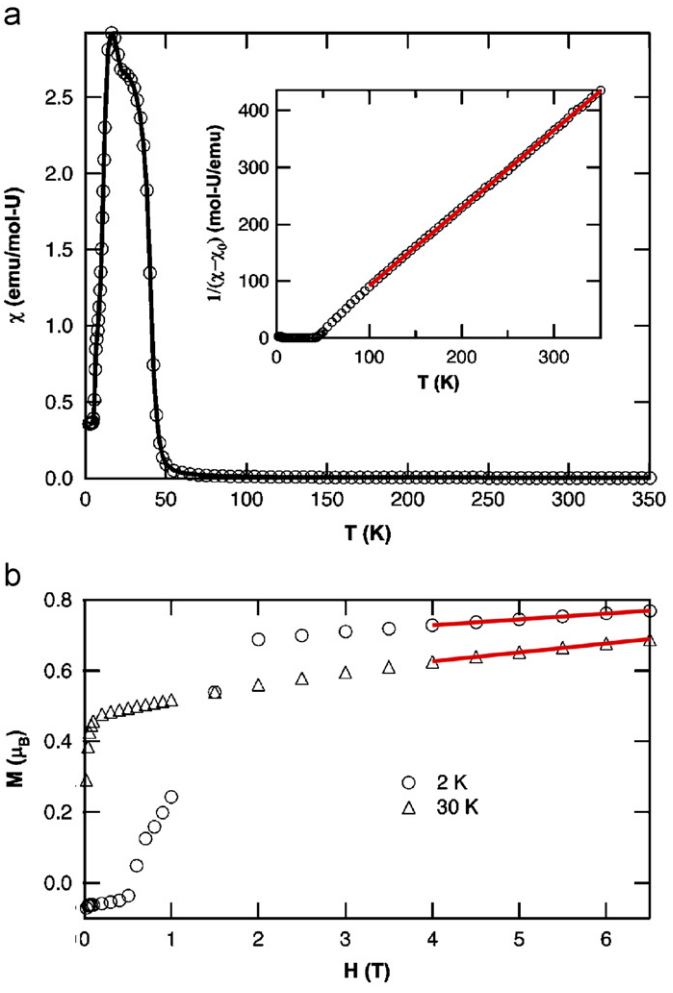

Fig. 3. (a) Zero field-cooled magnetic susceptibility versus temperature, normalized per mol-U. The inset shows the fit of the inverse susceptibility to the modified Curie–Weiss law $\chi = \chi_0 + C/(T-\Theta_{CW})$—the solid line above 100 K. (b) Magnetization versus applied magnetic field curves. Data obtained at 30 K are shown as triangles, data collected at 2 K are represented as open circles, respectively. The solid lines are the linear fits between 4 and 6.5 T.

tures), the reduced effective moment is in agreement with the reduced ordered moment in the magnetic state, consistent with at least partial itinerancy of the U moment. Similarly low effective moments are known for other U-intermetallics, for which the 5*f*-bands lie very close to the Fermi level and tend to be partially delocalized [1,12,21,27–31].

Below 100 K, two transitions can be identified by the inflection points of the susceptibility curve, and they are near 40 and 20 K, respectively. From the magnetization (M) as a function of the field (H) plots depicted in Fig. 3b, it can be deduced that the system enters into a ferromagnetic state at $T_1 \approx 40$ K, and that a spin reorientation possibly occurs at $T_2 \approx 20$ K. We note here that our data cannot rule out the possibility that the transition at 40 K is actually ferrimagnetic instead of ferromagnetic. The magnitudes of the moments, extracted by the zero field intercept of linear fits of the M versus H curves in Fig. 3b (fitted above 4 T), 0.53 μ_B at 30 K, and 0.66 μ_B at 2 K, clearly suggests that the magnetism involves local moments. In order to recover the full moment however, we would expect a transition with increasing field above the accessible range in our measurements.

The presence of two transitions in $U_3Co_2Ge_7$ was further confirmed by specific heat measurements shown in Fig. 4. The ferromagnetic transition at 40 K is smeared out by a magnetic field applied as expected, and the 20 K transition is no longer visible at 9 T. By plotting C_p/T versus T^2 as it is done in Fig. 5, one can extract the electronic contribution to the specific heat by the zero temperature intercept (aka γ or the Sommerfeld coefficient). A fit of the specific heat data to the form: $C_p = \gamma T + \beta T^3 + \alpha T^5$ results in $\gamma = 87$, 84, 85, and 81 mJ/mol-U K^2 for $H = 0$, 1, 3, and 9 T, respectively. In addition, $\beta = 0.53$, 0.61, 0.51, and 0.62 mJ/mol-U K^4 and $\alpha = 0.0030$, 0.0023, 0.0029, and 0.0015 mJ/mol-U K^6, each for 0, 1, 3, and 9 T, respectively. From the β-coefficient, the Debye temperature can also be extracted: $\theta_D = 244$ K in zero field. In a pure Debye model [37,38], this would imply that the lattice contribution exceeds the total measured heat capacity at higher temperatures. However, a pure Debye model is likely an oversimplification for fitting the entire lattice contribution. More importantly, we are probably overestimating the lattice contribution at low temperatures by neglecting a magnetic spin wave contribution, which could not be extracted at this time. A non-magnetic analog such as $La_3Co_2Ge_7$ and/or $Th_3Co_2Ge_7$ is needed, but attempts to synthesize such compounds have been unsuccessful so far.

Fig. 6 shows the temperature dependence of the electrical resistivity of $U_3Co_2Ge_7$. The resistivity at room temperature is $\rho_{295} = 220\ \mu\Omega$ cm—about two and half orders of magnitude higher than the resistivities of pure noble metals. A pronounced change in slope coincides with the onset of the first ferromagnetic transition, as expected. This is seen more clearly in the derivative plot illustrated in Fig. 7a. In $\delta\rho/\delta T$, the second transition is also visible. To determine the electron–electron scattering expected for a Fermi liquid we plot ρ versus T^2 in the inset of Fig. 6. A fit

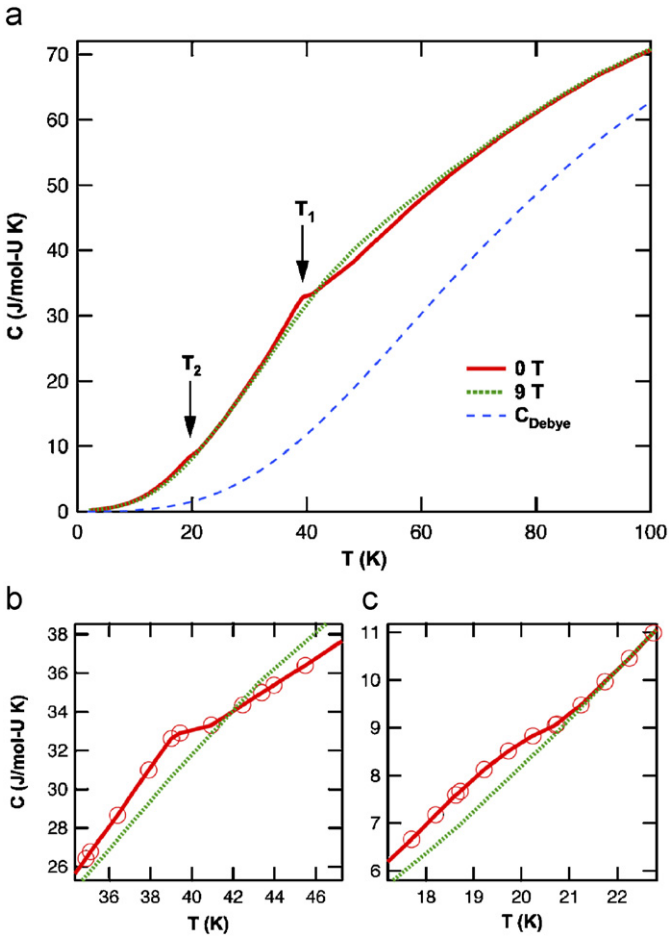

Fig. 4. (a) Specific heat of $U_3Co_2Ge_7$ versus temperature. The anomalies in the $C_p(T)$ data due to the two transitions are indicated by arrows. Magnified views centered at 40 and 20 K are depicted in (b) and (c), respectively. The thin dashed line in (a) is a simple Debye estimate of the lattice contribution with $\theta_D = 350$ K as described in the text.

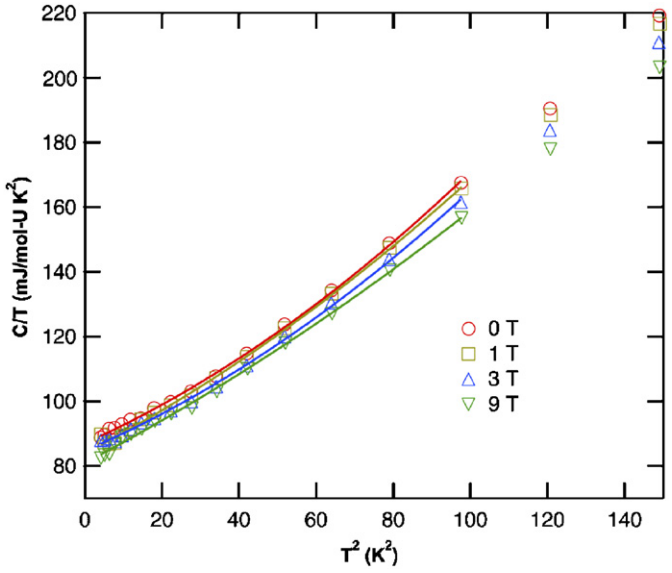

Fig. 5. Sommerfeld coefficient ($\gamma = C_P/T$) versus T^2. Solid lines are fits to $C_P = \gamma T + \beta T^3 + \alpha T^5$—see text for details.

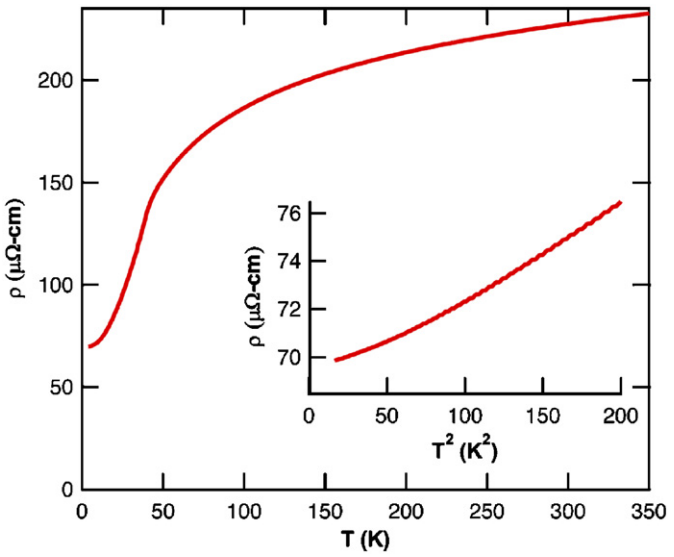

Fig. 6. Main panel: Resistivity versus temperature for single-crystal of $U_3Co_2Ge_7$. The direction of the applied current is presumed to be parallel to the direction of the fastest crystal growth, i.e., along the a and the c-crystallographic axes. Inset: resistivity versus T^2 in an attempt to extract the contribution of electron–electron scattering.

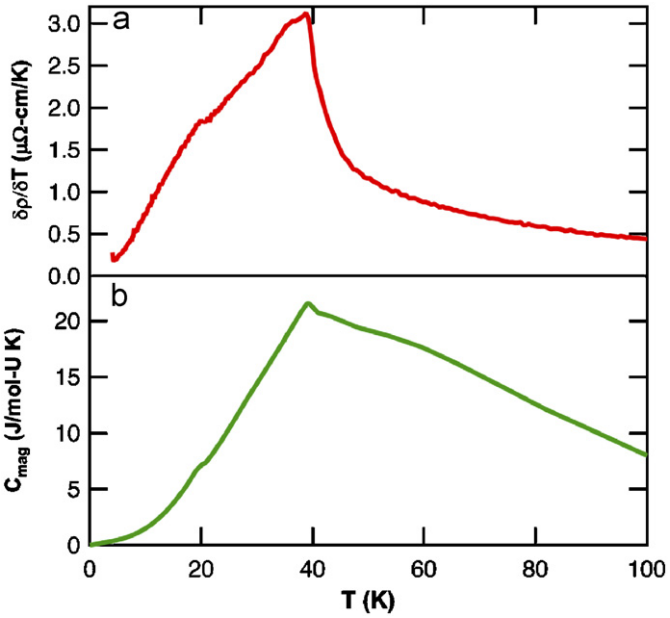

Fig. 7. Plots of $\delta\rho/\delta T$ (a) and C_{mag} (b) versus the temperature. C_{mag} is obtained by subtracting the lattice contribution expected from a Debye model with $\theta_D = 350$ K shown as the thin dashed line in Fig. 4.

of the data below 14 K to $\rho = \rho_0 + AT^2 + BT^4$ gives $\rho_0 = 69.4\,\mu\Omega\,\text{cm}$, $A = 0.023\,\mu\Omega\,\text{cm/K}^2$, and $B = 6.6 \times 10^{-5}$ $\mu\Omega\,\text{cm/K}^4$. Comparing the A-coefficient from the resistivity to the γ-coefficient from specific heat (i.e., C_P/T vs. T^2) we find a reasonable agreement with the phenomenological Kadowaki–Woods relation [39]. This gives us confidence in assigning the coefficient A to electron–electron scattering, and provides reasonable evidence that the ground state is a magnetic Fermi liquid. The T^4-contribution to resistivity possibly originates from magnetic scattering, or electron–phonon scattering (as we get nearly an equally good fit to $\rho = \rho_0 + AT^2 + BT^5$ expected for electrons scattering off of impurities, electrons, and phonons independently).

The above comparison of specific heat and resistivity in the form of the Kadowaki–Woods relation essentially stems from expectations based on Fermi liquid theory near $T = 0$ K [6,12]. Another comparison can be made at high temperatures by comparing the magnetic contribution to the specific heat C_{mag} to $\delta\rho_{mag}/\delta T$. Fisher and Langer have demonstrated that the leading term in the magnetic specific heat as well as in $\delta\rho_{mag}/\delta T$ is proportional to the spin–spin correlation function just above T_C [40]. Richard and Geldart later showed that this holds below T_C as well as above T_C [41]. We extracted the magnetic contribution to the specific heat by assuming a Debye contribution for the lattice, where we adjusted the Debye temperature $\theta_D = 350$ K, so as to give a reasonably smooth extrapolation for C_{mag} at high temperatures. This lattice contribution is shown by a thin dashed line in Fig. 4. Such a simple estimate of the phonon contribution gives a magnetic entropy which is too large, but alternative phonon subtractions give qualitatively similar results. Without the data for a non-magnetic analog we can also only plot $\delta\rho/\delta T$ instead of $\delta\rho_{mag}/\delta T$· Despite these shortcomings, one can readily see from Fig. 7 that both quantities are similar over a wide range of temperatures.

4. Conclusions

Reported were comprehensive structural and physical properties studies of single crystals of a new ternary compound $U_3Co_2Ge_7$. It crystallizes with the orthorhombic $La_3Co_2Sn_7$ type [18] and the structure has been unequivocally established by refinements from single-crystal X-ray diffraction data. $U_3Co_2Ge_7$ structure is devoid of disorder and/or flux inclusion and has two crystallographically unique uranium atoms, occupying sites with very different coordination. Due to the different U-atom environments, an intriguing possibility is that the ion in one uranium sites exhibit more localized (and magnetically ordered behavior), while the U-ions in the other site are more itinerant, similar to $U_3Ni_5Al_{19}$ [42]. The large nearest neighbor U–U distances of 3.878 Å and above are much greater than the Hill criterium of 3.4 Å [33], indicating a lack of significant f-wavefunction overlap, and hence one would expect the f-moments to be somewhat more localized. However, given the moderately large effective mass deduced from specific heat and resistivity measurements as well as the reduced moment value from susceptibility we anticipate that the uranium f-electrons hybridize with the p- and d-electrons from germanium and cobalt (to a lesser extent, as judged from the corresponding distances). Similar observations and conclusions were found in other uranium cobalt germanides such as $U_3Co_4Ge_7$, which is not too surprising given the similarities in the compositions and the crystal structures as discussed

above [21]. Our results show that $U_3Co_2Ge_7$ is a moderate heavy-fermion ferromagnet (ferrimagnet) at 40 K that undergoes another transition at 20 K, the nature of which is still under investigation.

Acknowledgments

Svilen Bobev acknowledges financial support from the University of Delaware through start-up funds. Work at LANL was performed under the auspices of the US DOE, Office of Science. The authors also acknowledge fruitful discussions with Dr. T. Park (LANL). We are indebted to the anonymous reviewer who pointed to us several unintentionally omitted references.

References

[1] (a) Reviews: (a) K.A. Gschneidner Jr., L. Eyring (Eds.), Handbook on the Physics and Chemistry of Rare Earths, vols. 1, 2, 17, 19, North-Holland, Amsterdam, 1978;
(b) M.B. Maple, Ø. Fischer, H.F. Braun (Eds.), Superconductivity in Ternary Compounds II: Superconductivity and Magnetism, Springer, Berlin, 1982;
(c) H.R. Ott, Z. Fisk, in: A.J. Freeman, G.H. Lander (Eds.), Handbook on the Physical and Chemistry of Actinides, vol. 5, North-Holland, Amsterdam, 1987, pp. 85–147;
(d) K.H.J. Buschow (Ed.), Concise Encyclopedia of Magnetic and Superconducting Materials, Elsevier, Amsterdam, 2005 and the references therein.
[2] Z. Fisk, H.R. Ott, T.M. Rice, J.L. Smith, Nature 320 (1986) 124.
[3] D.D. Koelling, B.D. Dunlap, G.W. Crabtree, Phys. Rev. B 31 (1985) 4966.
[4] Z. Fisk, H.R. Ott, J.L. Smith, J. Less-Common Met. 133 (1987) 99.
[5] Z. Fisk, D.W. Hess, C.J. Pethick, D. Pines, J.L. Smith, J.D. Thompson, J.O. Willis, Science 239 (1988) 33.
[6] J.D. Thompson, J.L. Sarrao, N.J. Curro, E.D. Bauer, L.A. Morales, F. Wastin, J. Rebizant, J.C. Griveau, P. Boulet, E. Colineau, G.H. Lander, Superconductivity in actinide materials, in: R. Alvarez, N.D. Bryan, I. May (Eds.), Recent Advances in Actinide Science, Royal Society of Chemistry, Cambridge, 2006, p. 680.
[7] S.S. Saxena, P. Agarwal, K. Ahilan, F.M. Grosche, R.K.W. Haselwimmer, M.J. Steiner, E. Pugh, I.R. Walker, S.R. Julian, P. Monthoux, G.G. Lonzarich, A. Huxley, I. Sheikin, D. Braithwaite, J. Flouquet, Nature 406 (2000) 587.
[8] G.R. Stewart, Z. Fisk, J.O. Willis, J.L. Smith, Phys. Rev. Lett. 52 (1984) 679.
[9] H.R. Ott, H. Rudiger, Z. Fisk, J.L. Smith, Phys. Rev. Lett. 50 (1983) 1595.
[10] Z. Fisk, G.R. Stewart, J.O. Willis, H.R. Ott, F. Hulliger, Phys. Rev. B 30 (1984) 6360.
[11] H.R. Ott, H. Rudiger, P. Delsing, Z. Fisk, Phys. Rev. Lett. 52 (1984) 1551.
[12] G.R. Stewart, Rev. Mod. Phys. 56 (1984) 755.
[13] P.W. Anderson, Phys. Rev. 124 (1961) 41.
[14] K.B. Blagoev, J.R. Engelbrecht, K.S. Bedell, Phys. Rev. Lett. 82 (1999) 133.
[15] C. Broholm, J.K. Kjems, W.J.L. Buyers, P. Matthewes, T.T.M. Palstra, A.A. Menovsky, J.A. Mydosh, Phys. Rev. Lett. 58 (1987) 1467.
[16] F. Levy, I. Sheikin, B. Greiner, A.D. Huxley, Science 309 (2005) 1343.
[17] (a) P.C. Canfield, Z. Fisk, Philos. Mag. B 65 (1992) 1117;
(b) M.G. Kanatzidis, R. Pöttgen, W. Jeitschko, Angew. Chem. Int. Ed. 44 (2005) 6996.
[18] P. Villars, L.D. Calvert (Eds.), Pearson's Handbook of Crystallographic Data for Intermetallic Compounds, second ed, American Society for Metals, Materials Park, OH, USA, 1991 and the desktop edition 1997.
[19] W. Dörrscheidt, H. Schäfer, J. Less Common Met 70 (1980) P1.
[20] (a) L.G. Akselrud, Y.P. Yarmolyuk, I.V. Rozhdestvensky, E.I. Gladushevsky, Kristallografiya (in Russian) 26 (1981) 186;
(b) D. Berthebaud, E.B. Lopes, O. Tougait, A.P. Gonçalves, M. Potel, H. Noël, J. Alloys Compds. 442 (2007) 348.
[21] R. Pöttgen, B. Chevalier, P. Gravereau, B. Darriet, W. Jeitschko, J. Etourneau, J. Solid State Chem. 115 (1995) 247.
[22] JADE Version 6.5, Materials Data, Inc., Livermore, CA, 2003.
[23] Bruker SMART and SAINT, Bruker AXS Inc., Madison, WI, USA, 2002.
[24] G.M. Sheldrick, SADABS, University of Göttingen, Germany, 2003.
[25] G.M. Sheldrick, SHELXTL, University of Göttingen, Germany, 2001.
[26] L. Durivault, F. Bouree, B. Chevalier, G. Andre, J. Etourneau, O. Isnard, J. Magn. Magn. Mater. 232 (2001) 139.
[27] (a) R. Troc, V.H. Tran, J. Magn. Magn. Mater. 73 (1988) 289;
(b) K.H.J. Buschow, E. Brück, R.G. van Wierst, F.R. de Boer, L. Havela, V. Sechovsky, P. Nozar, E. Sugiara, M. Ono, M. Date, A. Yamagishi, J. Appl. Phys. 67 (1990) 5215;
(c) A.M. Alsmadi, V. Sechovsky, A.H. Lacerda, K. Prokes, J. Kamarad, E. Brück, S. Chang, M.H. Jung, H. Nakotte, J. Appl. Phys. 91 (2002) 8123.
[28] (a) M. Kuznietz, H. Pinto, H. Ettedgui, M. Melamud, Phys. Rev. B 40 (1989) 7328;
(b) T. Endstra, G.J. Nieuwenhuys, A.A. Menovsky, J.A. Mydosh, J. Appl. Phys. 69 (1991) 4816;
(c) E. Hickey, B. Chevalier, B. Lepine, J. Etourneau, M.A.-F. Amos, J.F. da Silva, M.M. Amado, J.B. Sousa, J. Alloys Compds. 178 (1992) 413.
[29] W. Buchholz, H.-U. Schuster, Z. Anorg. Allg. Chem. 482 (1981) 40.
[30] B. Chevalier, P. Gravereau, T. Berlureau, L. Fournes, J. Etourneau, J. Alloys Compds. 233 (1996) 174.
[31] (a) P. Boulet, M. Potel, G. André, P. Rogl, H. Noël, J. Alloys Compds. 283 (1999) 41;
(b) P. Boulet, M. Potel, J.C. Levet, H. Noël, J. Alloys Compds. 262–3 (1997) 229;
(c) P. Boulet, A. Daoudi, M. Potel, H. Noël, J. Solid State Chem. 129 (1997) 113;
(d) P. Boulet, A. Daoudi, M. Potel, H. Noël, G.M. Gross, G. André, F. Bourée, J. Alloys Compds. 247 (1997) 104.
[32] C.S. Barrett, M.H. Mueller, R.L. Hitterman, Phys. Rev. 29 (1963) 625.
[33] H.H. Hill, in: W.N. Miner (Ed.), Plutonium and Other Actinides, The Metallurgical Society of AIME, New York, 1970.
[34] G. Venturini, I. Ijjaali, B. Malaman, J. Alloys Compds. 285 (1999) 194.
[35] S.E. Latturner, M.G. Kanatzidis, Chem. Commun. 18 (2003) 2340.
[36] E.I. Gladyshevskii, O.I. Bodak, V.K. Pecharsky, Mendeleev Chem. J. 30 (1985) 35.
[37] J.S. Smart, Effective Field Theories of Magnetism, Saunders, Philadelphia, PA, 1966.
[38] (a) S. Blundell, Magnetism in Condensed Matter, Oxford University Press, Oxford, UK, 2001;
(b) C. Kittel, Introduction to Solid State Physics, seventh ed, Wiley, Hoboken, NJ, 1996.
[39] K. Kadowaki, S.B. Woods, Solid State Commun. 58 (1986) 507.
[40] M. Fisher, J.S. Langer, Phys. Rev. Lett. 20 (1968) 665.
[41] T.G. Richard, D.J.W. Geldart, Phys. Rev. Lett. 30 (1973) 290.
[42] E.D. Bauer, V.A. Sidorov, S. Bobev, D.J. Mixson, J.D. Thompson, J.L. Sarrao, M.F. Hundley, Phys. Rev. B. 71 (2005) 014419.